Photogrammetry for Non-Invasive Terrestrial Position/Velocity Measurement of High-Flying Aircraft

Part V: Optical Encoder Completion & Transition to TI DSP

James A Crawford

Synopsis

Part I provided a simple introduction to the big-picture objectives for this multi-phase project.

Part II first looked at telescope mounts, ultimately focusing on the azimuth-elevation type mount for the project. The basic mathematics for dealing with 3-phase DC motors (e.g., Clarke and Park transformations) were introduced, along with the first ingredients for modeling and controlling the DC motors in a precision manner. The *Launchpad* hardware platform from Texas Instruments was selected to host the motor control algorithms.

In Part III, most of the attention was focused on the mechanical design, fabrication and assembly of the telescope mount. The detailed design of the hardware changed appreciably from the first concept as better approaches were recognized during the detailed design. A first-look at low rotational speed cogging torque was also conducted.

In Part IV, attention was directed to (i) the mechanical drive details for the elevation axis finally settling on a 25:1 belt-drive step-down approach and (ii) interfacing the optical encoders Table 2 *on the azimuth and elevation axes to an Arduino Mega2560 as an interim step to the TMS320F28379D digital signal processor.*

*In this portion of the project (*PART V*), work necessarily continued on the optical encoder because much of the project (e.g., motor control) depends upon securing a reliable optical encoder function. Excellent encoder performance was finally achieved after a 3rd design iteration of the encoder mount as described in §1.* The first real work with the Texas Instruments TMS320F28379D was also done, ultimately capturing all of the encoder functionality on this platform as initially done using the *Mega2560*. Near-term follow-up objectives round out this installment of my project narrative.

1 First Order of Business- AEAT-9000 Optical Encoder Mount

This topic has haunted me now for much of 2020 as the first two design iterations proved less than satisfactory to me. The second iteration is described in §5 for project completeness, but in the end I had to move to yet a 3rd design iteration.

Although the 3rd iteration of the mechanical mount for the optical encoder is arguably over-kill, its performance is excellent as is its repeatability and ease of alignment!

As mentioned at the end of §5, most of my performance difficulties would have probably been solved had I moved to a single one-piece high quality 8 mm axle through the entire encoder mount, rather than utilizing a 3/8" axle which was also turned down to 8mm for the encoder wheel. Leaving nothing to chance, I also procured a much better axle for this design iteration. I also made notable improvements with the bearings in this design iteration. However, since no cost-sensitive plans are in the forecast, it is more important (to me) to have excellent performance with this 3rd design pass and be able to move on to other aspects of my project rather than go through a cost reduction exercise now.

Two views of the final mechanical design are shown in Figure 1 and Figure 2.

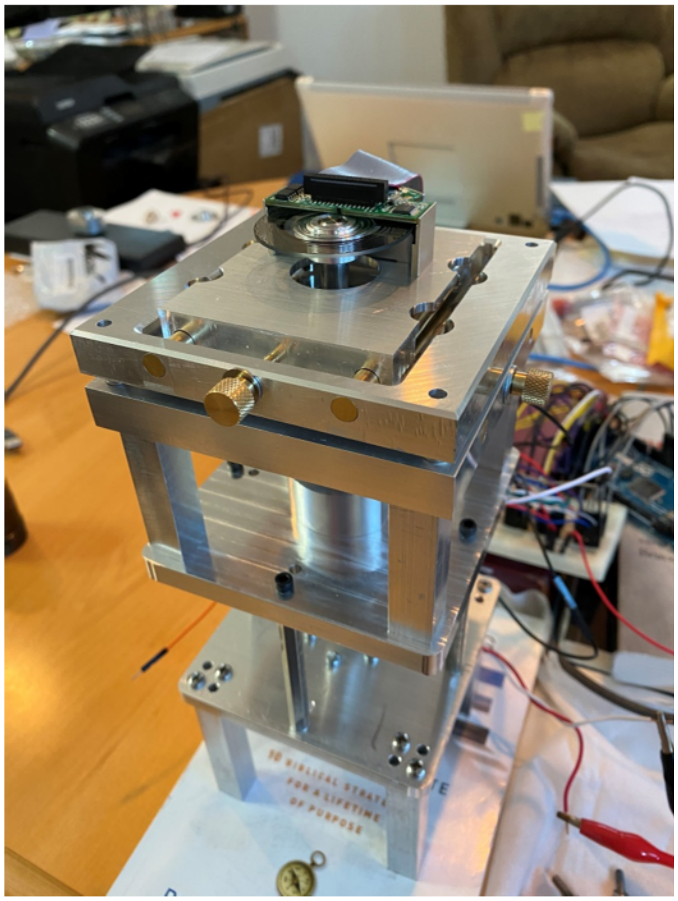
Figure 1 Gen3 encoder mount employing precision x-y positioner

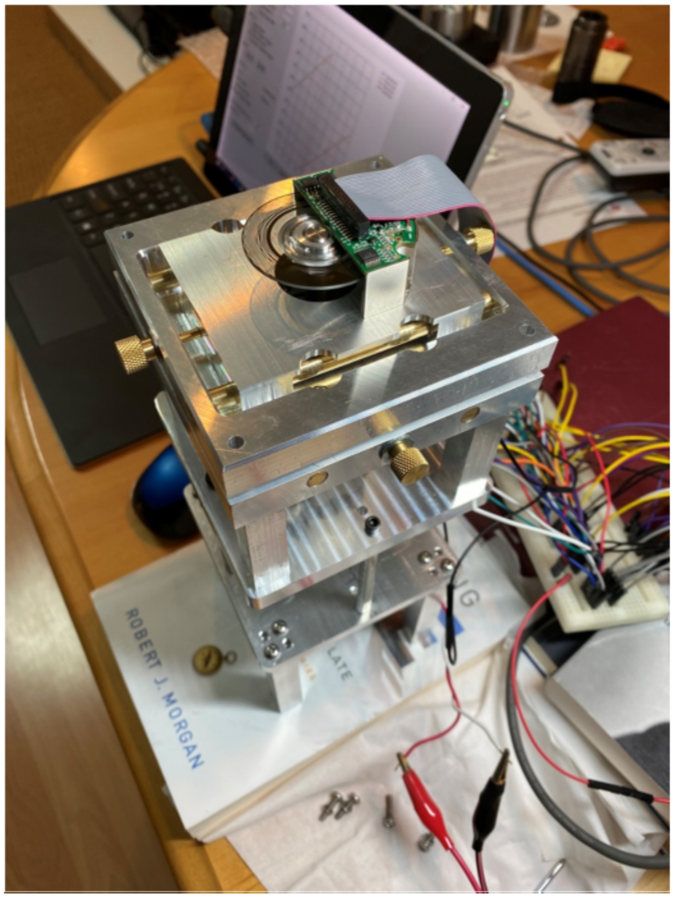
Figure 2 Secondary view of Figure 1

The new encoder mount using the precision x-y positioner I designed and fabricated myself is extremely easy to calibrate while also being rock solid and repeatable. Only the upper portion of the stack-up will be used on each of the telescope axes since the bottom half (consisting of a 12V DC 100 RPM motor and coupling) is present only for initial x-y positioner alignment purposes.

One of the major design objectives was to be able to align each optical encoder on this test jig, and then be able to move it directly to the telescope axes without having to touch the alignment a second time. By all indications, it looks like this objective has been achieved.

A protective housing over the encoder wheel and associated electronics will have to be fabricated of course to deal with environmental factors, but this design is otherwise completed and ready to move on to the next phases in the project.

1.1 Baby Steps with the Arduino Mega2560 Platform

A C# graphical user interface (GUI) was written with a full command protocol for communications between the PC and the Arduino Mega2560 which interfaces with the AEAT-9000 encoder. One of the diagnostic screen shots from this program is shown in Figure 3. This aspect was originally discussed in Part IV of this project story, but clean sawtooth behavior[1] was never really achieved because of the performance issues associated with the encoder mount. With the new encoder mount, pristine sawtooth behavior was always observed as shown in Figure 3.

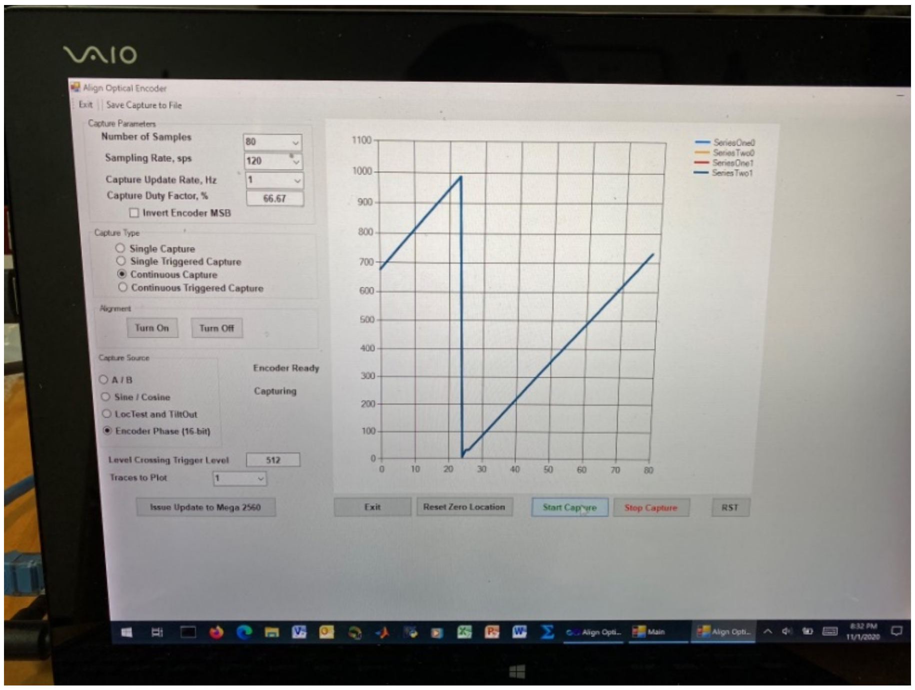

Number of Samples: 80
Sampling Rate, sps: 120
Capture Update Rate, Hz: 1
Capture Duty Factor, %: 66.67
☐ Invert Encoder MSB

Single Capture [✓ Continuous Capture] Single Triggered Capture Continuous Triggered Capture

A / B Sine / Cosine LocTest and TiltOut [✓ Encoder Phase (16-bit)]

Level Crossing Trigger Level: 512
Traces to Plot: 1

Figure 3 16-bit absolute phase versus time from the encoder using a motor RPM value in the vicinity of 50. The ideal sawtooth wave is the result of a nearly constant RPM rate from the DC motor. A separate diagnostic screen is used to examine the LSB behavior with no motor rotation applied.

[1] A constant motor RPM results in a constant angular velocity, and consequently a constant slope of the encoder angle versus time.

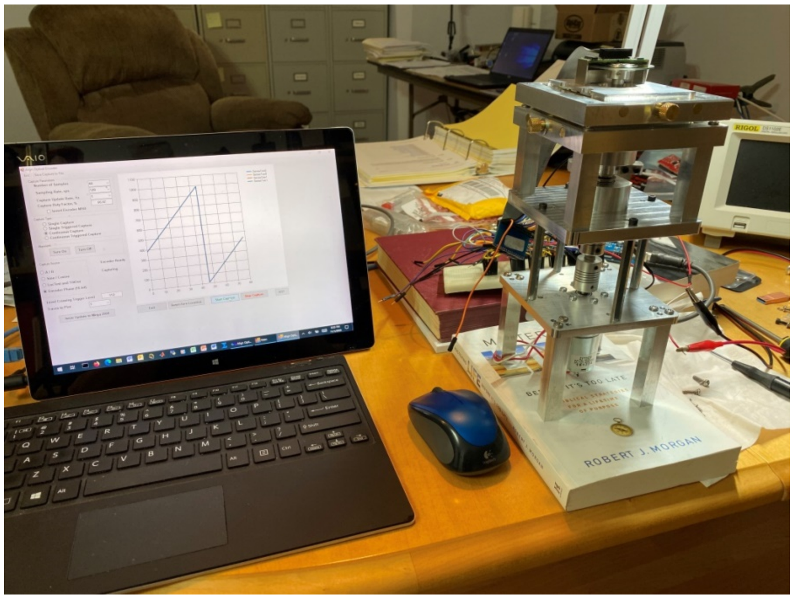
Figure 4 Wider perspective of encoder test jig operating with host PC and Arduino Mega

2 TMS320F28379D-Centric Activities

Closure of the optical encoder mount design is finally enabling other aspects of this project to get underway. A second encoder mount remains to be built and the two encoders physically integrated with the telescope's azimuth and elevation axes. Progress on the 25:1 torque enhancement block for the elevation axis is nearing completion as well. Serious attention to the digital signal processing aspects of the project is finally being given and the *next steps* described in §5 of [4] the previous project installment pursued.

The near-term activities involving the DSP are sketched out in Figure 8. More specifically:

- new C# graphical user interface (GUI) was written to support new phase of project
- serial (asynchronous) communications between the host PC and DSP was developed, including a new command protocol
- serial communications between the DSP and optical encoder were developed based upon the lessons learned using the Arduino Mega2560
- control/interfacing between the DSP and its DRV8301 Booster Pack finished off the hardware aspects for this installment

Many additional tasks remain to be accomplished of course, but the divide-and-conquer approach outlined here was completed, with the next-steps described later in §3.

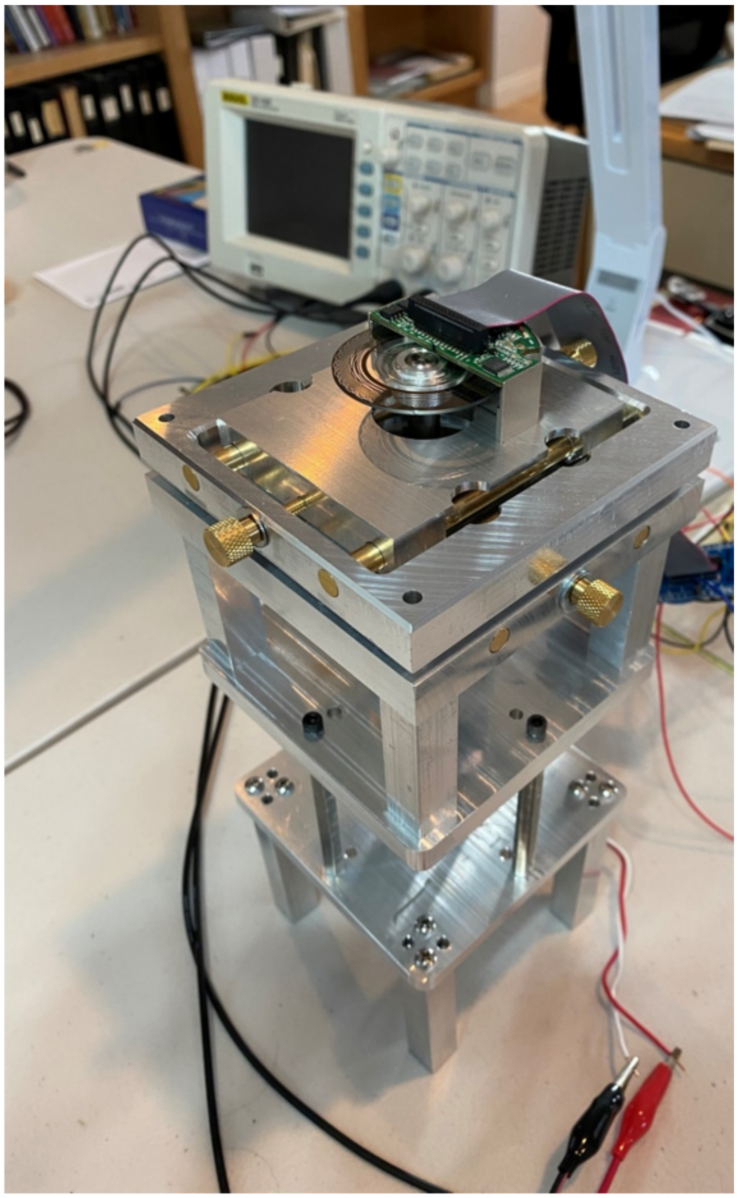
Figure 5 Optical encoder, precision xy positioner, radial and axial bearings, and test-jig low RPM motor. Only the top 1/3 of this assembly will be needed on each axle of the final telescope mount. (Mega2560 electronics)

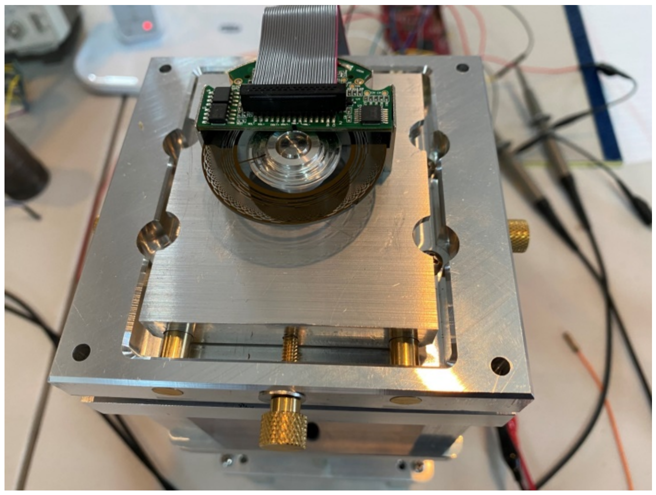
Figure 6 AEAT-9000 encoder and optical wheel. (Mega2560 electronics)

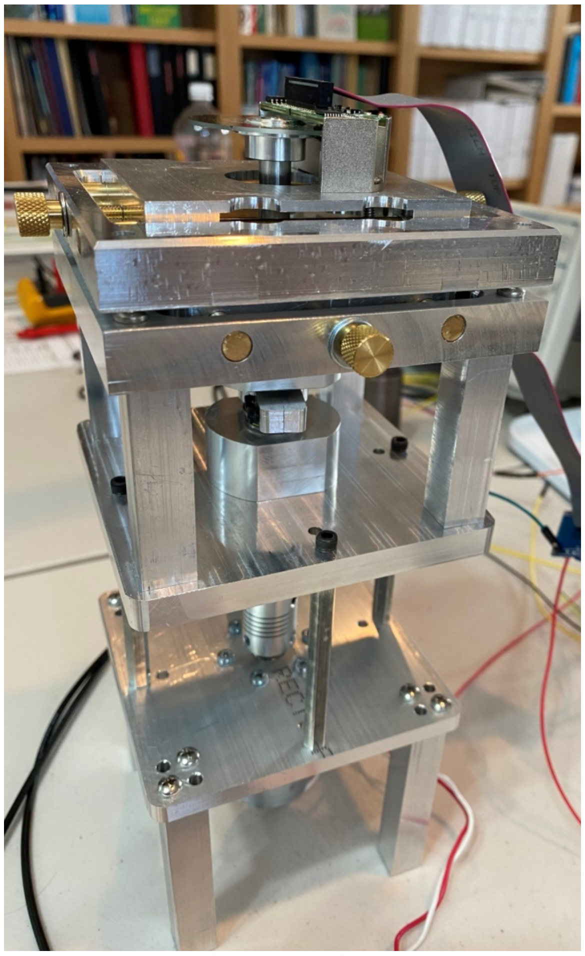
Figure 7 Side view of Figure 5. (Mega2560 electronics)

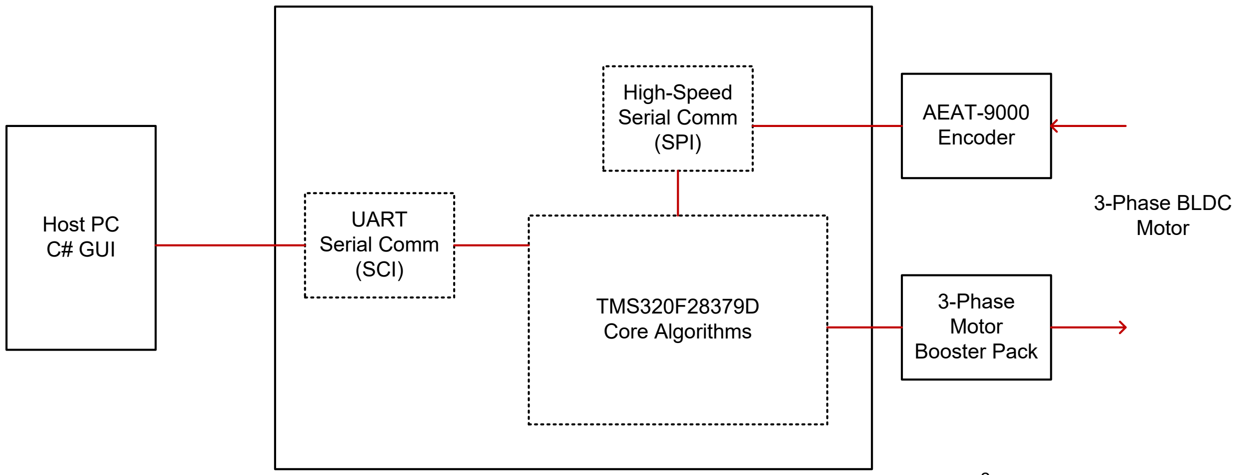

Figure 8 Major DSP elements involved with full motor control of one telescope axis[2]

2.1 Host PC GUI

The DSP must communicate with something during its related development so it is necessary to develop the host PC software along in parallel. The splash screen for the host PC as presently working is shown in Figure 9.

The *Diagnostics* box in the lower right-hand corner will largely duplicate the functionality which was previously implemented using the Arduino Mega2560 platform. The *Telescope Alignment* box in the lower left-hand corner addresses future calibration activities of the telescope mount which will be done against the night time background star field. A precision alignment method is crucial for the dual telescope alignment, and was anticipated from the very beginning of the project [1].

The *Control* diagnostics box middle-right will be the gateway into all of the brushless DC (BLDC) motor control elements which have only been touched on to-date. In general, a large amount of effort will be involved with each of the front-panel *button functions*, and these will be developed step by step as the project progresses.

[2] From U27313 DSP Related.vsd.

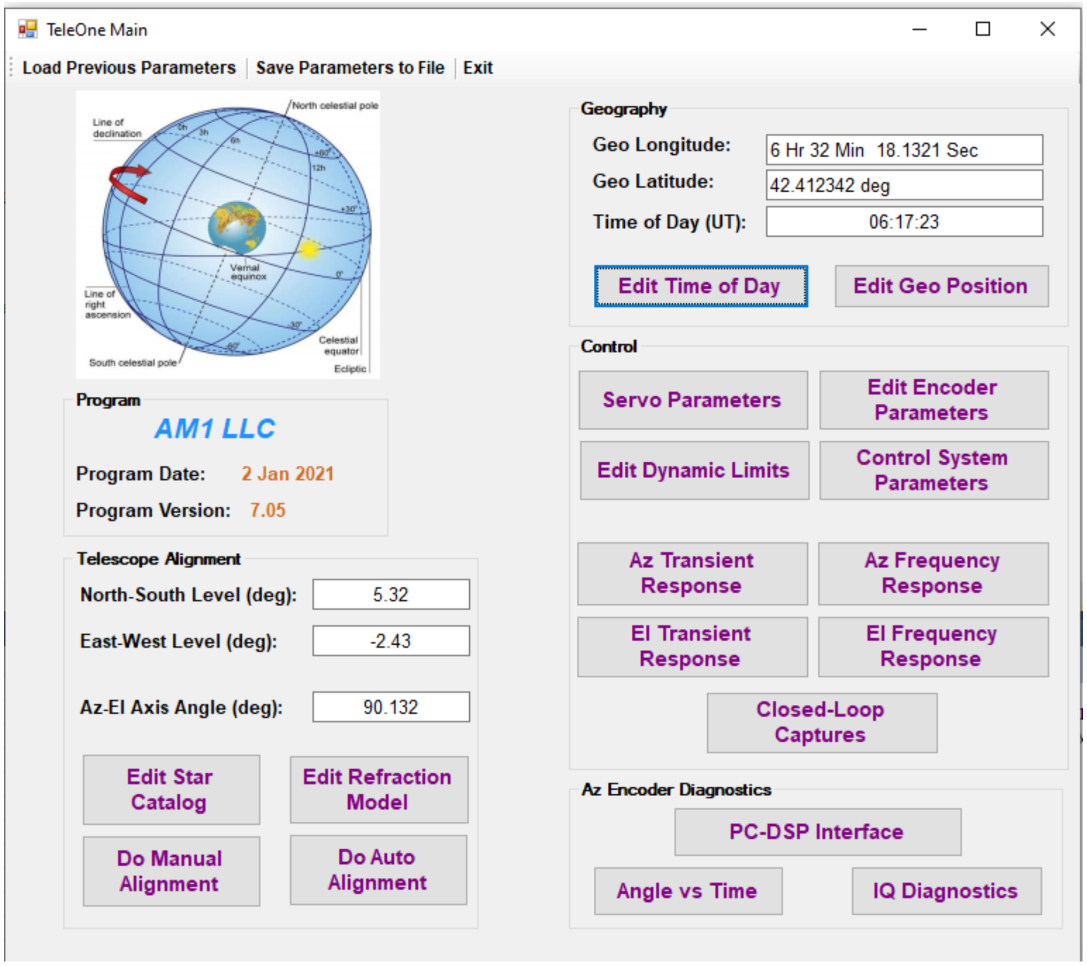

Program Date: 2 Jan 2021
Program Version: 7.05

North-South Level (deg): 5.32
East-West Level (deg): -2.43
Az-El Axis Angle (deg): 90.132

Geo Longitude: 6 Hr 32 Min 18.1321 Sec
Geo Latitude: 42.412342 deg
Time of Day (UT): 06:17:23

Figure 9 Splash screen for the new C# GUI

2.2 PC-DSP Serial Communications

This communication occurs between the PC's COM port and DSP's UART (COM) port. The DSP's SCI resources are used to support this communication.

Generally speaking, only one baud rate will be used. The port configuration is 8 data bits, 1 stop bit, and no parity. Testing has been done for the this interface at several baud rates up to as high as 460.8 kbps with zero errors observed over a 12.5 hour period (14.871e6 characters or 118.97e6 bits). An example screen shot of interface testing is shown in Figure 10. All communication via the COM port to the DSP will be done using ASCII text strings. Data requested from the DSP by the PC will generally be returned as 16-bit quantities using fixed formats.

The *PC-DSP Interface Diagnostics* splash screen is shown in Figure 10. As noted in the caption, extensive testing was done at 460.8 kbps with no errors observed. The speed for this interface needs to be chosen in conjunction with activities conducted via the DSP's SPI ports, however, to avoid excessive interrupt collisions. To this end, the tentative baud rate used for PC-DSP communications is 57.6 kbps whereas the baud rate used for SPI communications (with the AEAT-9000 optical encoders) is 4 Mbps.

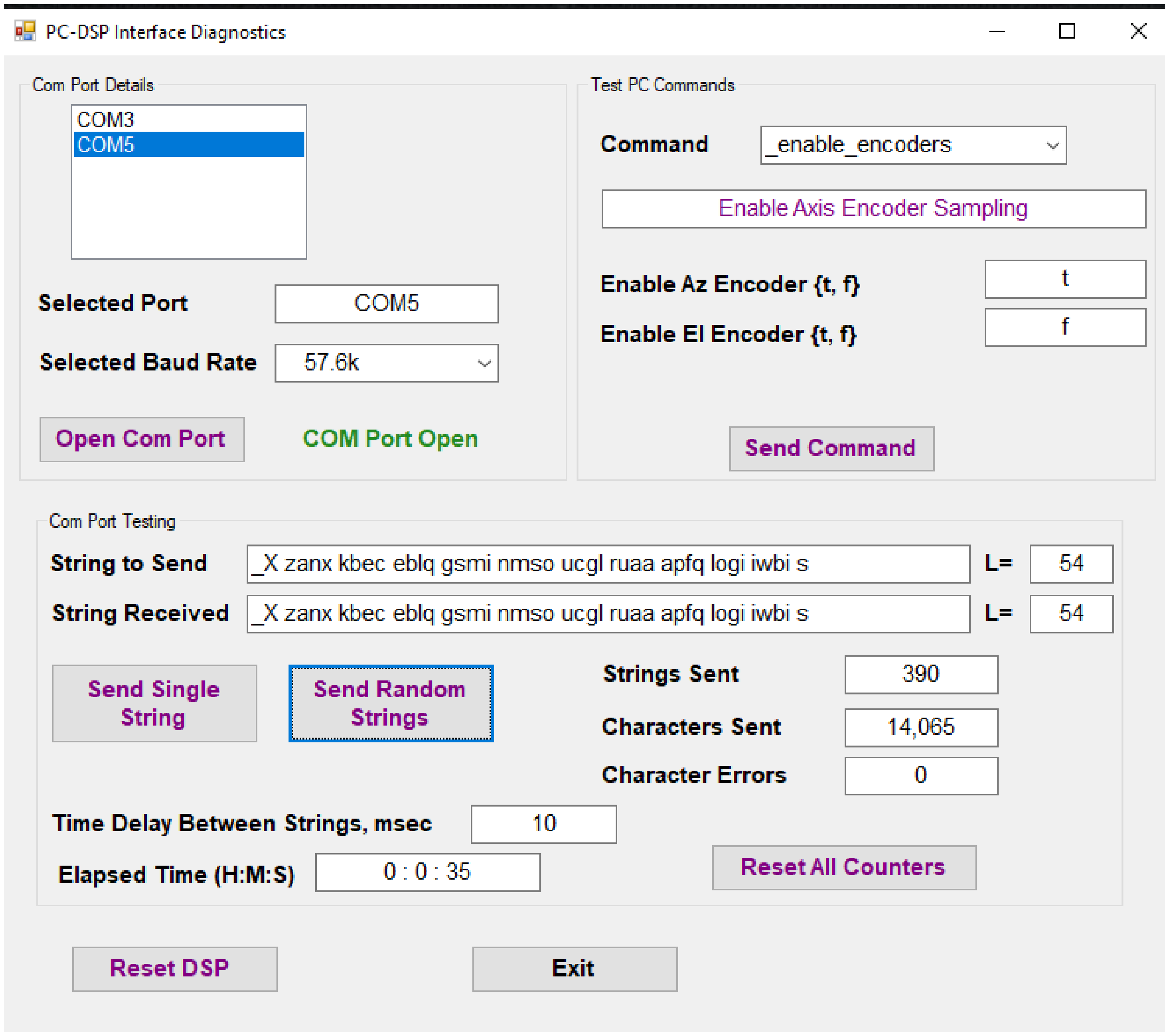
PC-DSP Interface Diagnostics

Com Port Details

COM3
COM5

Selected Port: COM5

Selected Baud Rate: 57.6k

COM Port Open

Test PC Commands

Command: _enable_encoders

Enable Axis Encoder Sampling

Enable Az Encoder {t, f}: t

Enable El Encoder {t, f}: f

Com Port Testing

String to Send: _X zanx kbec eblq gsmi nmso ucgl ruaa apfq logi iwbi s L= 54

String Received: _X zanx kbec eblq gsmi nmso ucgl ruaa apfq logi iwbi s L= 54

Strings Sent: 390

Characters Sent: 14,065

Character Errors: 0

Time Delay Between Strings, msec: 10

Elapsed Time (H:M:S): 0 : 0 : 35

Figure 10 Screen shot of the PC-DSP interface undergoing test. Running at 460.8 kbps, no errors observed over 12.5 hours and equivalently about 14.872 million characters[3]. String length is randomly varied from 8 characters up to 60 characters in length. The baud rate for the PC-DSP interface has tentatively been set at 57.6 kbps.

[3] SCI RXFIFO_RX2 for the interrupt, minimum string length = 1 character. Increasing FIFO interrupt level to RX8 (FIFO is 8/16 full before declaring interrupt) required a minimum string length of 10 characters.

2.2.1 PC to DSP Commands

All commands to the DSP from the PC will be done using ASCII strings which are terminated in one null character (0). Only the command string starting with "_X" is automatically echoed back from the DSP to the PC.

A PC-to-DSP command consists of (i) a command name and (ii) up to 3 subsequent parameter values all delineated by a white space. The command string must be terminated by a null character (0) as already mentioned. The available commands are listed in Table 1.

Table 1 PC-to-DSP Commands

Command	Description	Parameter 1	Parameter 2	Parameter 3
$$$$	DSP reset			
_reset_dsp	DSP reset			
_X	Dummy message to be echoed back to PC from 8 to 40 characters long	message		
_set_az_limits	Set limits for azimuth axis range, deg	+limit	-limit	
_set_el_limits	Set limits for elevation axis range, deg, relative to horizontal	+limit	-limit	
_set_az_slew_limits	Limit azimuth slew rate, deg/sec	+limit	-limit	
_set_el_slew_limits	Limit elevation slew rate, deg/sec	+limit	-limit	
_reset_encoders	Issue reset signal to encoders	az reset	el reset	
_zero_encoders	Set 0^o position for azimuth and or elevation encoders	az true/false	el true/false	
_enable_encoders	Start sampling action for azimuth and or elevation encoders	az enable	el enable	
_set_loop_fs	Set sampling rate to be used by both control loops, sps	f_s		
_set_pwm_mash	Set order (0,1,2) for azimuth and elevation MASH Δ-Σ algorithm	az value	el value	
_enable_pwms	Enable azimuth and or elevation axis PWM	az enable	el enable	
_set_az_pid_gains	Set azimuth control loop proportional, integral, and differential gains	proportional	integral	differential
_set_el_pid_gains	Set elevation control loop proportional, integral, and differential gains	proportional	integral	differential
_setup_az_hr_observer	Set up gain parameters for high-rate azimuth $\theta_{encoder}(t)$ observer	α	β	
_setup_az_lr_observer	Set up gain parameters for low-rate azimuth $\theta_{encoder}(t)$ observer	α	β	
_setup_el_hr_observer	Set up gain parameters for high-rate azimuth $\theta_{encoder}(t)$ observer	α	β	
_setup_el_lr_observer	Set up gain parameters for low-rate azimuth $\theta_{encoder}(t)$ observer	α	β	
_encoder_location	Trap on encoder encountering location mark	*az_on*	*el_on*	

Command	Description	Parameter 1	Parameter 2	Parameter 3
_setup_az_pwm	Setup parameters for azimuth PWM			
_setup_el_pwm	Setup parameters for elevation PWM			
_setup_capture[4]	Setup to read parameters with decimation factor and block size	*deci*	*blk_size*	*cap_type*
_do_capture	Initiate a capture (one-time) "a" for Az, "e" for El; "o" or "c"	*az_or_el*	*open_or_closed loop*	
_close_loops	Close control loops, {t, f}	*az_loop*	*el_loop*	
_step_az_axis	Step azimuth axis given amount	$d\theta$		
_step_el_axis	Step elevation axis given amount	$d\theta$		
_point_to	Point telescope to specified az/el angles	*az_angle*	*el_angle*	

Electrical interfacing details for operating the AEAT-9000 with the Arduino MEGA2560 were provided in an earlier report [4]. These interfacing details are repeated here for convenience in Table 3 of §5. Only a subset of these signals can be supported in the full-up DSP version supporting full servo control because (i) the DRV8301 Booster Pack (which will drive the two 3-phase motors) will take up a large number of I/O pins and (ii) two optical encoders need to be supported as well. Two configurations were used for this portion of the project:

- **Configuration 1:** Run the TMS320F28379D *without* the DRV8301's present to free up more GPIO pins for general I/O. This configuration supported all of the functionality provided in the Arduino version.
- **Configuration 2:** Install the DRV8301 Booster Packs on the DSP, and retain as much of the 1st configuration functionality as possible. With only one DRV8301 installed, all of the 1st configuration functionality has been retained.

2.2.2 SCI Interface (DSP $\leftrightarrow$ PC)

The F28379D's SCIA interface is used for communications between the PC and DSP. The baud rate for this interface should not be chosen independently of the encoder sampling rate because the SCI interface can only be serviced / checked at this sampling rate. If the encoder sampling rate is too low and the SCI baud rate too high, the SCIA FIFO may be overrun. Tentatively:

SCI baud rate = 57.6 kbps
SPI baud rate = 4 Mbps
Encoder sampling rate= 8 kHz to 160 kHz[5]

All communications from the PC to the DSP are ASCII strings. Data returned from the DSP is, however, functionally dependent and generally binary in nature to conserve throughput. Blocks of data associated with the encoders' angular position or (*I, Q*) signals are sent back from the DSP to the PC upon command. These quantities are always sent as 16-bit signed integer quantities.

[4] 0: do nothing, 1: open-loop, angle data; 2: open-loop, I/Q data; 3: closed-loop
[5] This rate easily supported without closed-loop calculations included yet. This high rate does demonstrate, however, the proficiency of the optical encoder and DSP-encoder interface routines.

2.2.3 Dedicated GPIO (DSP ↔ Encoder)

The optical encoders (AEAT-9000) require several dedicated control signals from the DSP aside from the SPI interface. Port SPIA is dedicated to azimuth operations and SPIB will be dedicated to elevation operations.

Table 2 DSP ↔ AEAT-9000 Encoder Interface. Full (I/Q) support is only shown for the azimuth channel.

DSP Signal Name	DSP GPIO	DSP Pin	Encoder Signal Name	Flex-Cable Pin
SPIACLKA	60	J1-7	SCL	**28**
SPISIMOA	58	J2-15		
SPISOMIA	59	J2-14	Dout+	**22**
SPISTEA	61	J2-19	NSL	**14**
ZRSTA	122	J2-17	zero_Reset	12
nRSTA	123	J2-18	nRST	26
COSINEAP	ADCINA0	J3-30	COSINE+	1
COSINEAN	ADCINB2	J3-28	COSINE-	2
SINEAP	ADCINC3	J3-24	SINE+	3
SINEAN	ADCIN14	J3-23	SINE-	4
SPIACLKB	65	J5-47	SCL	
SPISIMOB	63	J6-55		
SPISOMIB	64	J6-54	Dout+	
SPISTEB	66	J6-59	NSL	
ZRSTB			zero_Reset	
nRSTB			nRST	
+5VA		J3-21		27, 29
GNDA		J3-22		6, 8, 17, 18
+5VB		J7-61		
GNDB		J7-62		

One issue did come up in formulating the interface details shown in Table 2. Although the AEAT-9000 datasheet clearly stated SCL- and NSL- signal inputs can be tied to fixed rail voltages and the device operated effectively single-ended, this was not the case. In order for proper operation to occur, SCL- and NSL- signals had to be tied to approximately VCC/2.

Once each encoder is installed into the telescope mount, only 3-wires (plus power and ground) should be required to communicate with the AEAT-9000's as highlighted in bold-blue Flex-Cable Pin numbers as shown in the table.

The SPI configuration adopted (from CodeComposer) is given by

```
SPI_setConfig(SPIA_BASE, DEVICE_LSPCLK_FREQ, SPI_PROT_POL1PHA0,
              SPI_MODE_MASTER, 4000000, 16);
SPI_disableLoopback(SPIA_BASE);
      SPI_setEmulationMode(SPIA_BASE, SPI_EMULATION_STOP_AFTER_TRANSMIT);
```

This information provides the polarity and phasing used for the 3-wire interfacing, along with the 4 Mbps baud rate and 16-bits per word details.

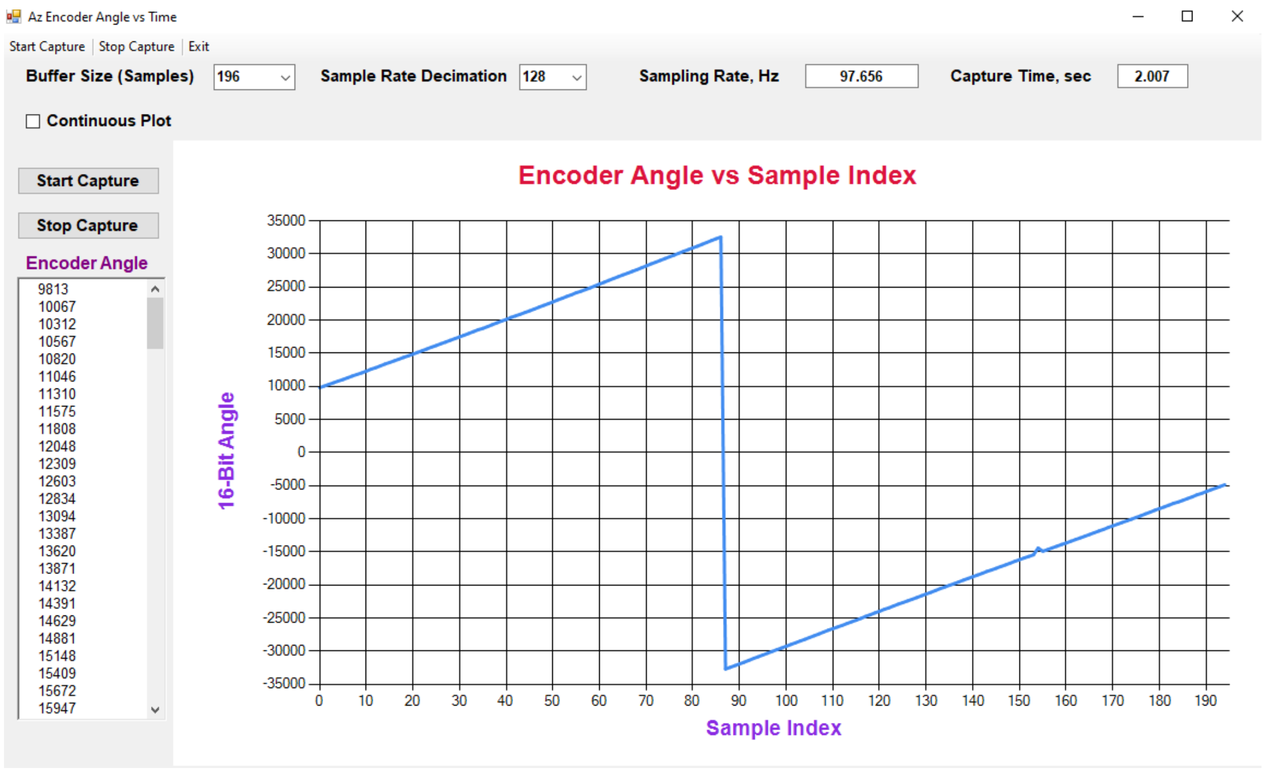

Buffer Size (Samples) 196 Sample Rate Decimation 128 Sampling Rate, Hz 97.656 Capture Time, sec 2.007

Encoder Angle

```
9813
10067
10312
10567
10820
11046
11310
11575
11808
12048
12309
12603
12834
13094
13387
13620
13871
14132
14391
14629
14881
15148
15409
15672
15947
```

Figure 11 Encoder phase versus time plot for constant RPM case

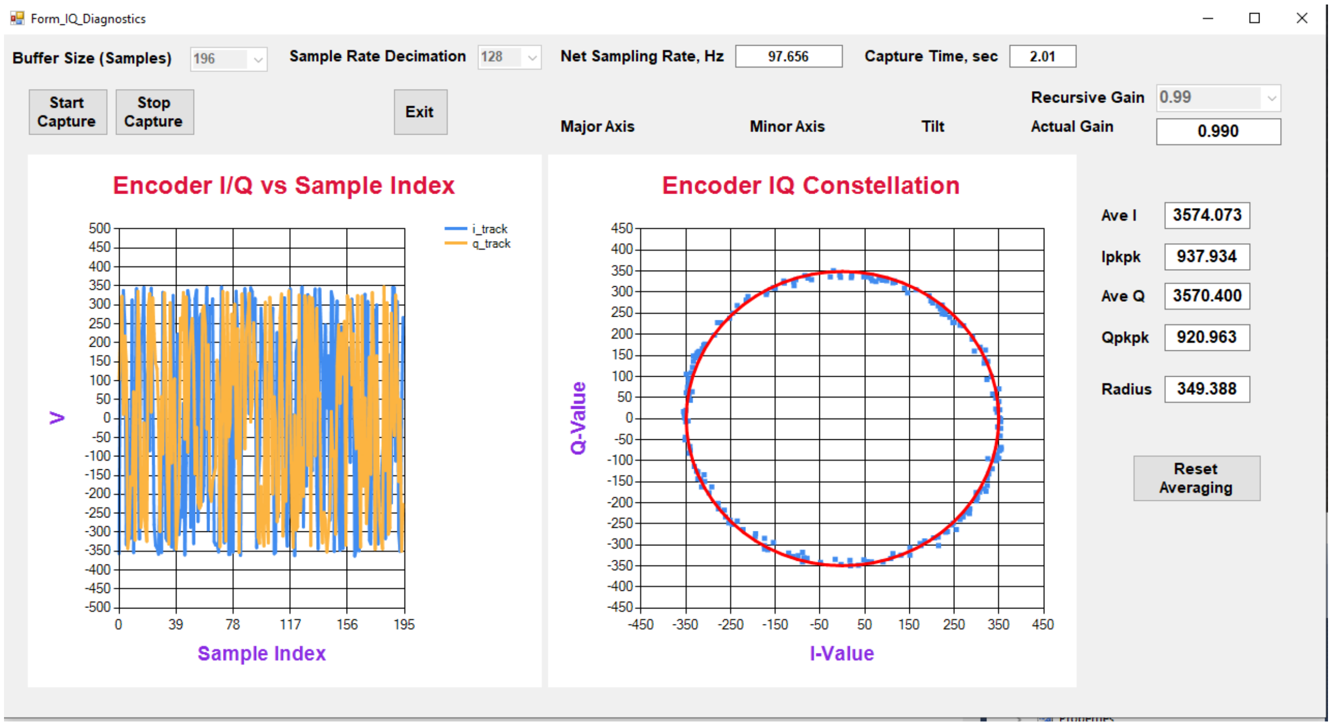

Buffer Size (Samples) 196 Sample Rate Decimation 128 Net Sampling Rate, Hz 97.656 Capture Time, sec 2.01

Recursive Gain 0.99

Major Axis Minor Axis Tilt Actual Gain 0.990

Ave I	3574.073
Ipkpk	937.934
Ave Q	3570.400
Qpkpk	920.963
Radius	349.388

Figure 12 Analog interpolation using quadrature waveforms is used within the decoder to extend angular resolution from 11-bits to 17-bits. The constellation plot assists with the fine-alignment step.IQ sample values should fall along the perimeter of a best-fit circle as shown here in the right-hand plot.

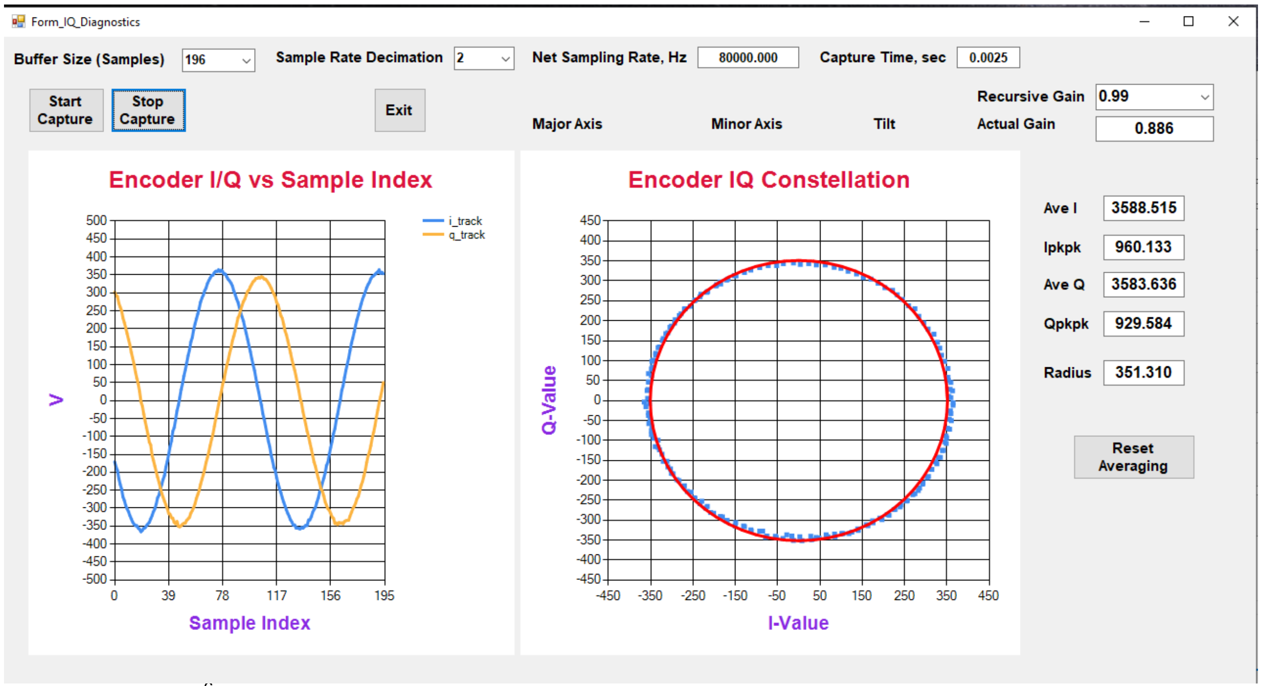

Buffer Size (Samples) 196
Sample Rate Decimation 2
Net Sampling Rate, Hz 80000.000
Capture Time, sec 0.0025
Recursive Gain 0.99
Actual Gain 0.886
Major Axis
Minor Axis
Tilt
Ave I 3588.515
Ipkpk 960.133
Ave Q 3583.636
Qpkpk 929.584
Radius 351.310

Figure 13 Same[6] as Figure 12 except encoder sampling rate increased from 12.5 kHz to 160 ksps using a post-sampling decimation factor of 2

Figure 12 and Figure 13 provide some insight into how well the optical encoder is aligned. Since the optical encoders will primarily be utilized for estimating position (thereby entailing essentially zero radian frequency), the quality of the signal I,Q constellation versus angle is what is of greatest interest. This information can only be obtained by using a fairly high encoder sampling rate and from which this perspective is stitched together.

The slowest rotational rate my nominal 100 RPM motor can spin at without stalling is roughly 30 RPM. One cycle of the interpolating I,Q sinewaves occurs between each of the 2048 *ticks* on the encoder wheel. Consequently, the sinewave frequency at this lowest RPM rate is on the order of (30/60)*2048 = 1024 Hz. Therefore, an encoder sampling rate of at least 32,768 sps is required in order to have roughly 32 samples per sinewave period.

Different encoder sampling rates combined with different sample buffer depths can be used to explore the numerical precision of the encoder's performance. As described in §8, a constant angular velocity presumption is made. Several known encoder wheel imperfections are known to be present and these are manifested as larger spikes in Figure 14 and Figure 15. The RMS error (relative to a straight line) appears to be independent of the sample rate and capture window width. The encoder is known to be extremely sensitive so the RMS floor of about 12 LSBs is presently believed to be due to angular roughness of the (very inexpensive) low RPM motor since it has a substantial gear-reduction train built in. This assumption remains to be proven/disproven by other means.

[6] The AEAT-9000 creates the last 6-bits or resolution using analog interpolation of in-phase and quadrature-phase signals. This 90^o relationship can be seen in the left-hand graphic of the figure.

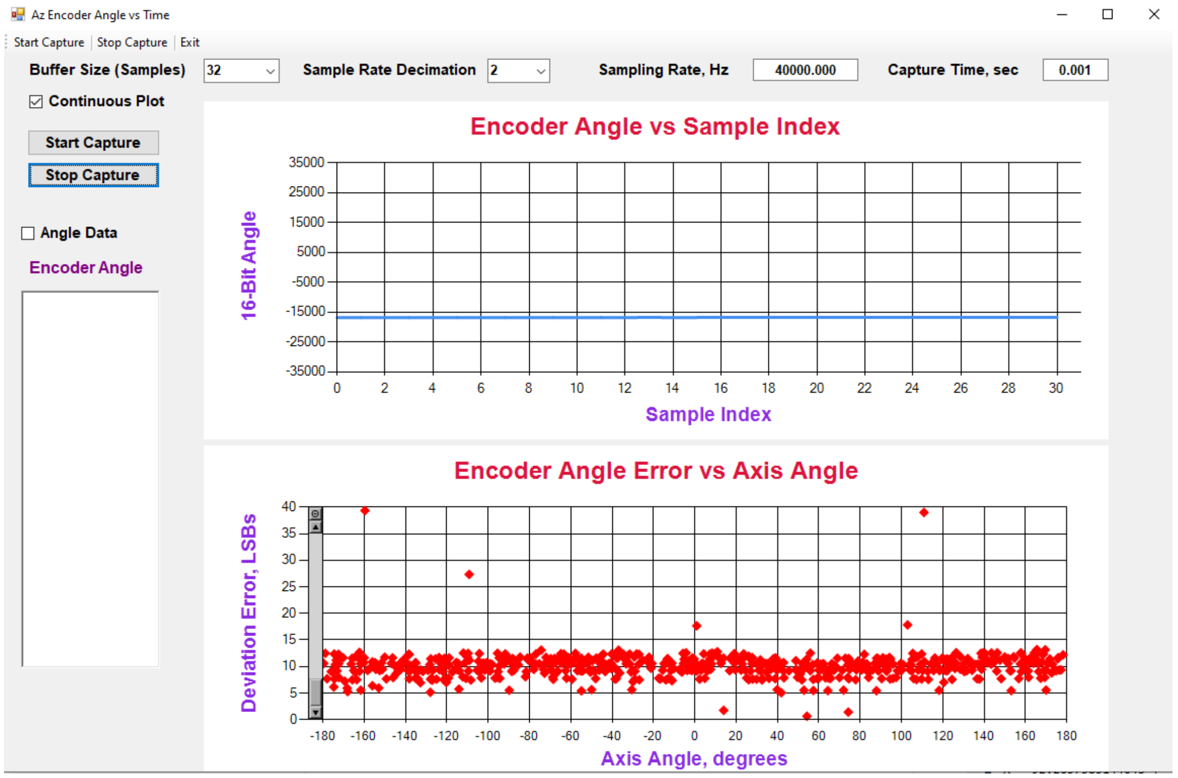

Buffer Size (Samples) 32 | Sample Rate Decimation 2 | Sampling Rate, Hz 40000.000 | Capture Time, sec 0.001

Figure 14 Decimated sampling rate of 40 ksps with sample capture interval of about 0.8 msec

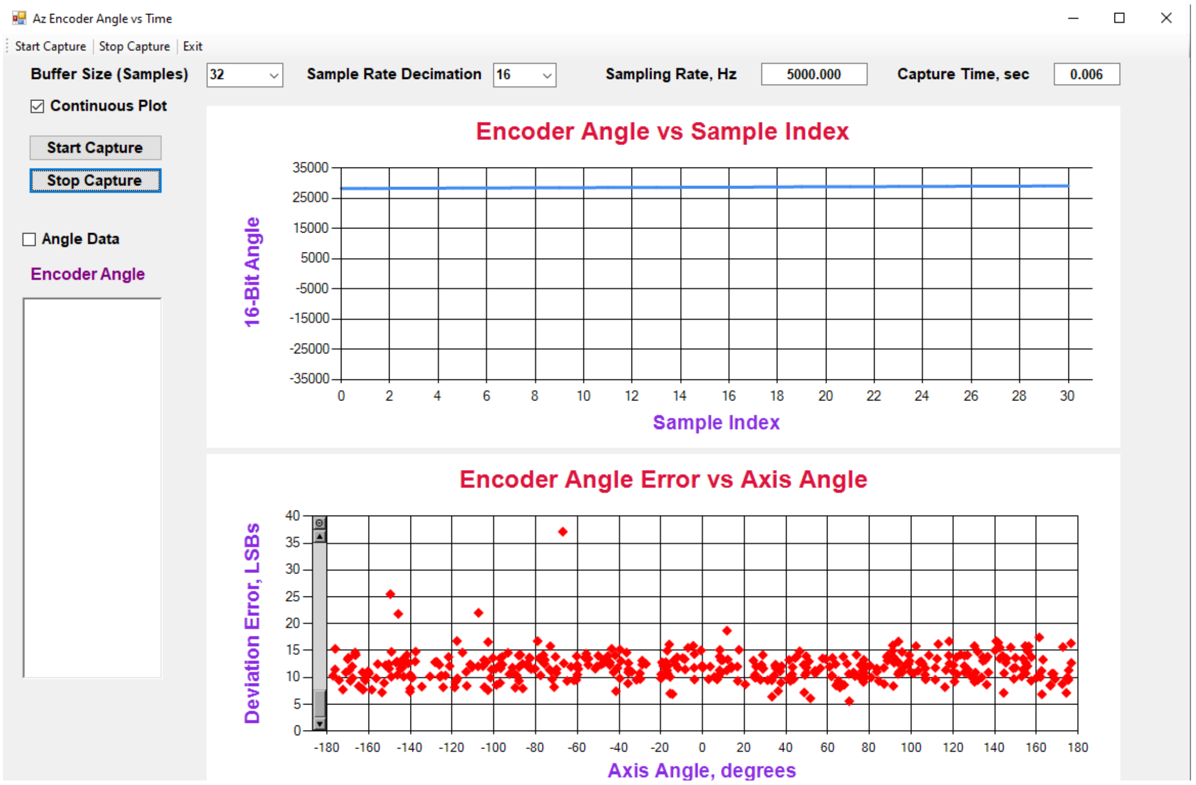

Buffer Size (Samples) 32 | Sample Rate Decimation 16 | Sampling Rate, Hz 5000.000 | Capture Time, sec 0.006

Figure 15 Decimated sampling rate of 5 ksps with sample capture interval of about 6.4 msec

2.3 Texas Instruments DRV8301 BLDC Motor Booster Pack

The Texas Instruments DRV8301 Booster Pack was easily installed atop the TMS320F28379D Launchpad. The DRV8301 provides 3.3V to the Launchpad, and a switcher on the Launchpad is used to create 5V for the Launchpad as well as the AEAT-9000 optical encoder. Jumpers had to be changed on the Launchpad as:

- Remover jumpers JP1, JP2, and JP3
- Install jumper JP6

The results shown in Figure 13 were taken with the hardware configured with the Booster Pack as discussed herein and shown in Figure 16.

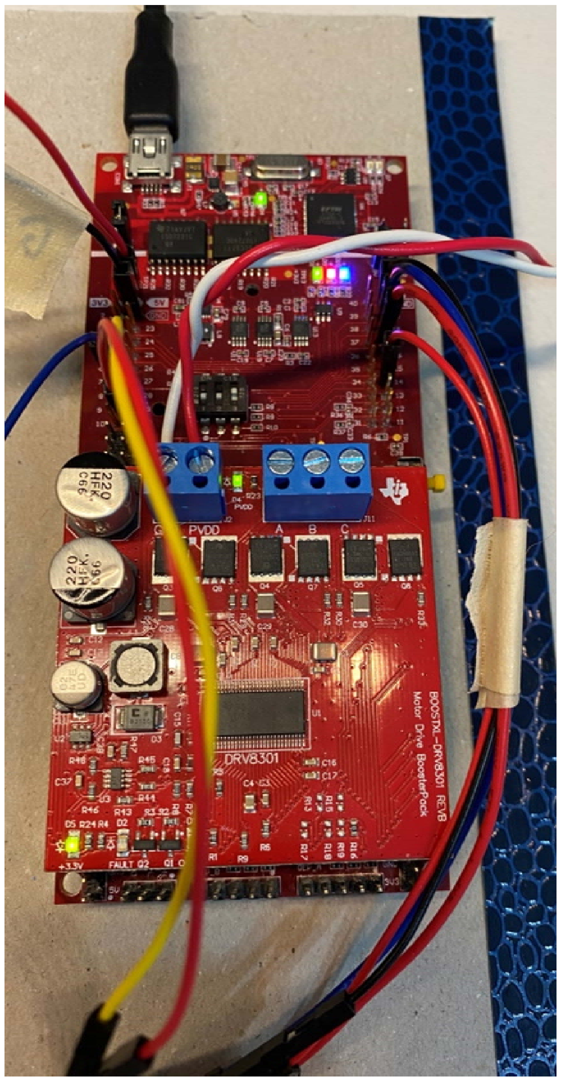

Figure 16 DRV8301 Booster Pack installed atop the TMS320F28379D Launchpad XL DSP board. The twisted red-white pair bring in +12V whereas other voltages (3.3V and 5V) are created internally.

3 Next Steps

Both hardware and software elements remain to be developed. With the encoder mounting now solved, there do not appear to be any major obstacles ahead on the hardware side (aside from possibly configuring the second DRV8301 atop the Launchpad XL and having sufficient IO).

On the software side, however, a great deal of work remains to be done. At this juncture, the most tedious appears to be proper configuration and usage of the ePWM blocks which are used to drive the 3-phase motors. The concepts involved are not difficult, but a fair amount of tedium is expected in getting the end-results to match expectations.

3.1 Near-Term Hardware Efforts

- Fabricate at least 2 more encoder mounts
- Design and fabricate test jig modification to replace 100 RPM motor with small 3-phase DC motor (planned for elevation axis less 25:1 pulley module) for algorithm development
- Design and fabricate encoder mount to azimuth axis assembly
- Complete the elevation 25:1 pulley module

3.2 Near-Term Software Efforts

- Become familiar with ePWM modules including all limit/safety features
- Become familiar with built-in control loop accelerator hardware (CLA) within the F28379D
- Code a first-cut rudimentary control loop

4 References

1. J.A. Crawford, “Photogrammetry for Non-Invasive Terrestrial Position/Velocity Measurement of High-Flying Aircraft,” Part I, 16 Oct. 2017, U24866.
2. ___________, “Photogrammetry for Non-Invasive Terrestrial Position/Velocity Measurement of High-Flying Aircraft, Direct-Drive Motors,” Part II, 23 April 2019, U24933.
3. ___________, “Photogrammetry for Non-Invasive Terrestrial Position/Velocity Measurement of High-Flying Aircraft, Direct-Drive Motor Chassis Design & Assembly,” Part III, 12 Nov 2019, U24933.
4. ___________, “Photogrammetry for Non-Invasive Terrestrial Position/Velocity Measurement of High-Flying Aircraft, Optical Encoder & Elevation Drive,” Part IV, 23 Aug 2020, U24933.
5. ____________, *Advanced Phase-Lock Applications- Synthesis*, Chapter 5, unpublished.

5 Appendix: Optical Encoder Work- 2nd Iteration

Work on the optical encoder (Broadcom AEAT-9000) has continued in the installment of the project. Unfortunately, this encoder was obsoleted by Broadcom mid-2020, but because its claimed 17-bit single-rotation precision is rather unique in the industry at this price-point, I decided to make a *lifetime buy* of devices for myself and press forward. Other encoders are available in the marketplace, but at a substantially higher price-tag (6x and higher).

Although the two-thumbwheel alignment concept from Part IV should have been sufficient conceptually speaking, device alignment proved to be almost impossible because this approach co-mingled x-axis and y-axis corrections. Not surprisingly, literally *everything* matters when it comes to getting the advertised performance from the device. Notably:

- rotational axis concentricity must be extremely good (better than 0.001") for the code wheel.
- vertical positioning of the codewheel between the AEAT9000's built-in LED and supporting sensors has been found to be very critical as well.
- x-dimension and y-dimension positioning must be rock solid, delivering consistent positioning with an accuracy (after alignment) on the order of 0.001"

I built a new-and-improved optical encoder alignment jig at the beginning of this project installment as shown in Figure 17

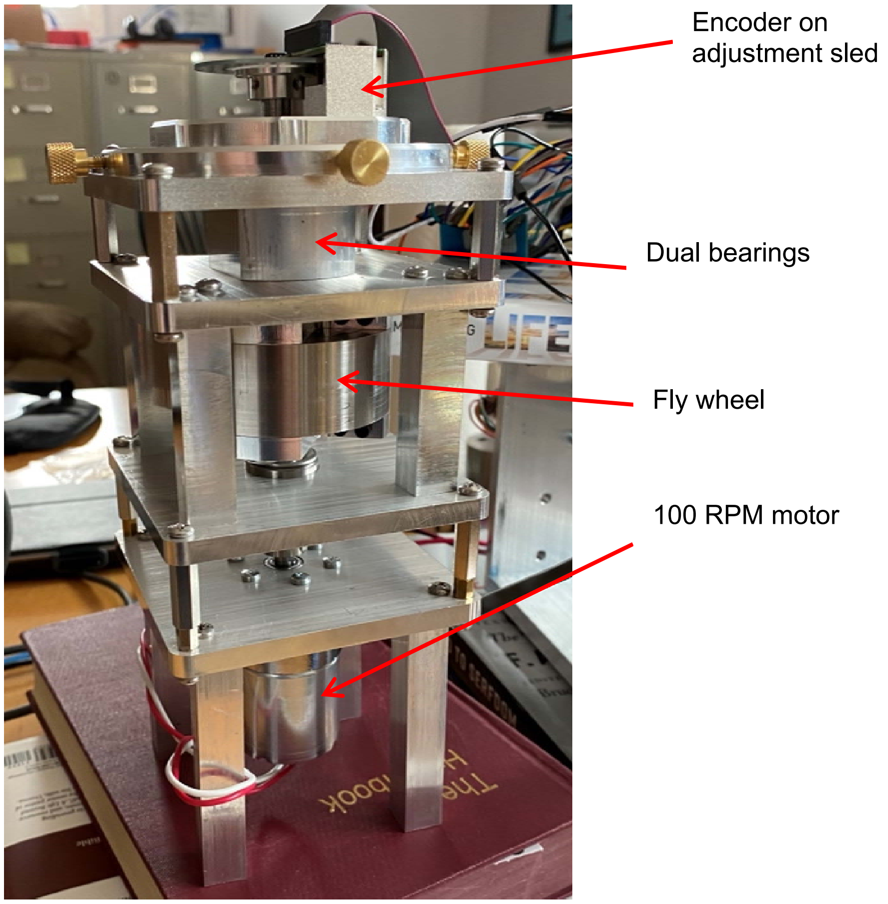

Figure 17 Revised optical encoder alignment-test jig

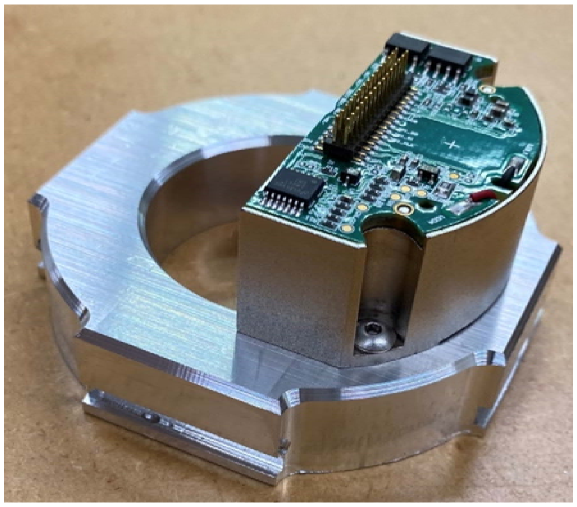
Figure 18 AEAT9000 optical encoder mounted on sled

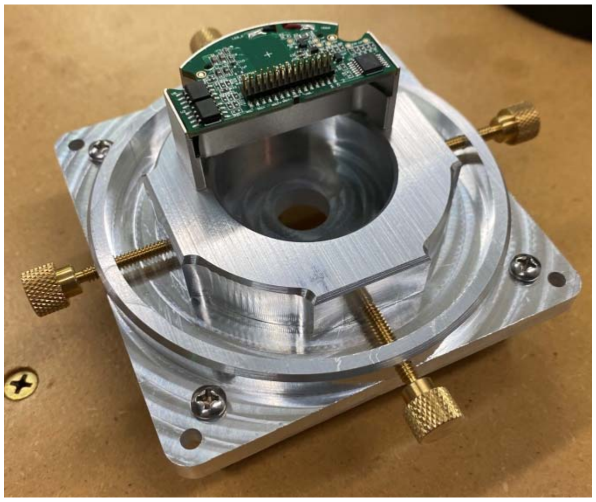
Figure 19 Sled situated in adjustment housing

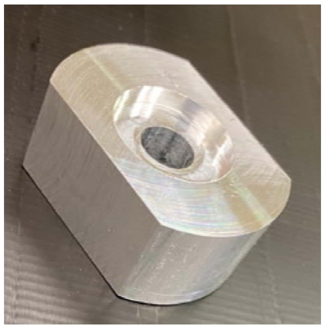
Figure 20 Milled housing for dual bearings

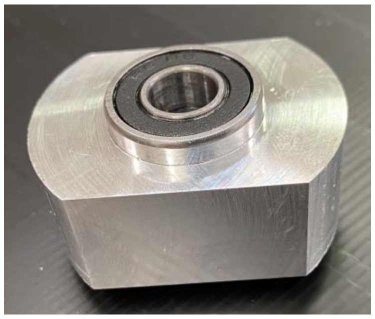
Figure 21 Housing with dual bearing installed-milled to a precision of about 0.0005”

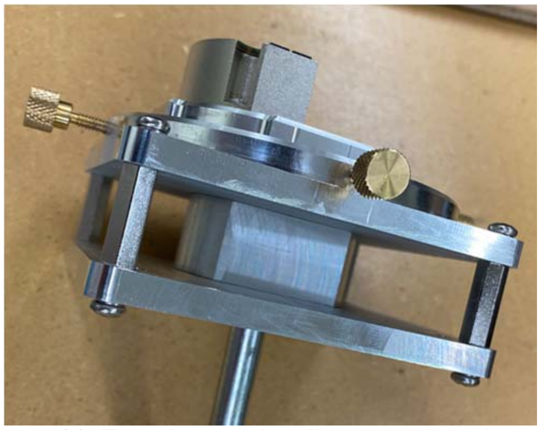
Figure 22 Encoder, sled, adjustment housing and dual bearings assembled together

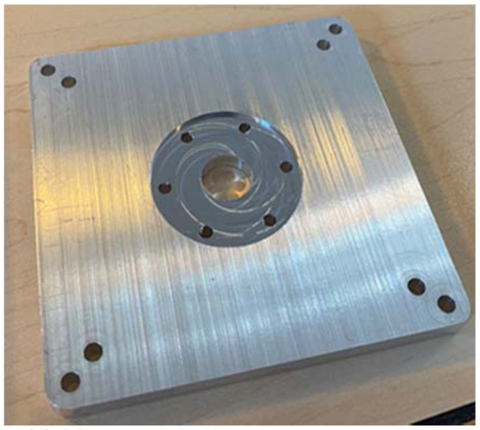
Figure 23 Motor mounting plate

Two additional photos of the completed alignment jig are shown in Figure 24 and Figure 25. I reached several other conclusions using this improved calibration jig:

- Even though I turned the axle on my lathe to a concentricity better than a few thousandths of an inch, I found the sloppiness in the bearings and axle-related concentricity still came through and resulted in an unacceptable amount of *wobble*.
- Bearing arrangement *must* address all three dimensions as already mentioned.
- A flex-coupling is probably recommended between the optical encoder assembly's rotational axis and the end application
- Precision alignment of the stand-alone assembled optical encoder should take place first, followed by mating of the assembly to the final application. Otherwise, in-situ alignment could be problematic.
- Using the 6-32 thumbscrews for x-y adjustment could probably have worked even with the backlash and poor rigidity during adjustment, but hoping to avoid yet another design iteration in the future, a better approach is needed.
- The exercise did validate the AEAT-9000'S claimed achievable performance at least to a degree. Mechanical integrity must still be improved, however, before a complete victory can be declared.

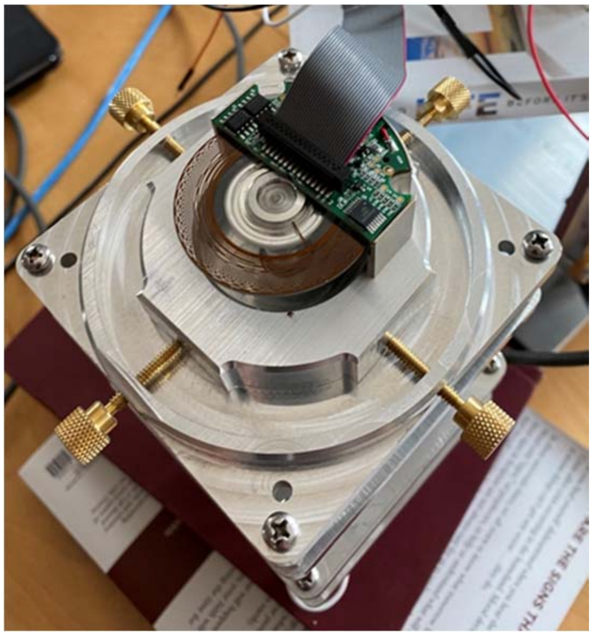
Figure 24 Top-view of alignment jig in action

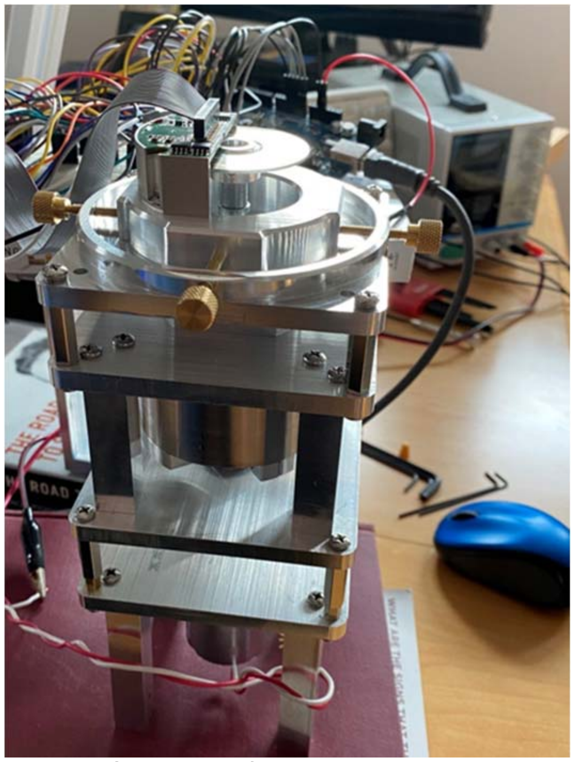
Figure 25 Side-view of alignment jig in action

Moving to the next level, I took the following steps:

1. Purchase high-precision bearings and axle components from McMaster-Carr.
2. Rather than use a 3/8" rod and have to turn the diameter down to 8mm to fit the code wheel's inner diameter, opt to use a 8mm diameter rod throughout the stand-alone optical encoder assembly.
3. A flexible coupler should be used to mate the stand-alone optical encoder assembly to its final application.
4. A much more rigid reproducible design for the x-y plane adjustments needs to be used.

Table 3 Optical Encoder I/O Mapping from AEAT-9000 to Arduino MEGA2560 [4] (Pin # refers to the flex cable wire index)

Encoder Pin Name	Pin #		Mega 2560 Pin Name	Dig/Ana	Mega I / O	Comments
COSINE+	1		A0	A	I	Truly differential
COSINE-	2		A1	A	I	Truly differential
SINE+	3		A2	A	I	Truly differential
SINE-	4		A3	A	I	Truly differential
TiltOut	5		22	D	I	Used for encoder/wheel tilt alignment. Two pulses per encoder revolution.
GND	6		Hard to GND			
LocTest	7		A4	A	I	Used for radial code wheel alignment
GND	8		Hard to GND			
Not Used	9		---			
MSBINV	10		23	D	O	
SPI_CLK	11		24	D	O	
Zero_RST	12		25	D	O	
SPI_SI	13		26	D	O	
NSL+	14		50	D	O	Connect to GND before encoder is powered on
SPI_SO	15		27	D	I	
NSL-	16		48			Connect to VDD before encoder is powered on
GND	17		Hard to GND			
GND	18		Hard to GND			
INCB	19		30	D	I	
DOUT-	20		47	D	I	
INCA	21		32	D	I	
DOUT+	22		33	D	I	
DIN-	23		38	D	O	
LERR	24		39	D	I	
DIN+	25		40	D	O	
nRST	26		41	D	O	Encoder reset
VDD	27		5V	PWR		
SCL+	28		42	D	O	
VDD	29		5V	PWR		
SCL-	30		43	D	O	

6 Appendix: Signal Observer

The DSP signal observer blocks perform filtering and signal conditioning within the system. The topic was first introduced in §4.1 of [2]. The observer's behavior is governed by two parameters denoted by α and β.

The DSP design makes use of low-rate and high-rate observer functions which are identical except for the (α, β) parameter values used. The high-rate observer block will generally be used within the control loops where additional signal delay must be kept to a minimum. The low-rate observer blocks are intended for use when monitoring of the system's behavior is of interest and the observer output is decimated down to rates on the order of 100 sps or less.

7 Appendix: 3-Phase Interpolation Algorithms

Unlike most motor control algorithms in the literature, I need to have very precise (e.g., 10 arc-second) precision pointing making jitter or wandering of either axis critical concerns. Since the associated algorithms must be executed at the sampling rate (i.e., perhaps as high as 160 ksps), execution efficiency is critical as well. Making use of the build-in CLA's within the F28379D should help ease memory as well as execution resource concerns.

For 3-phase control, the voltage waveforms given by

$$\begin{aligned} V_A &= A_A \sin(\theta) \\ V_B &= A_B \sin\left(\theta + \frac{4}{3}\pi\right) = A_B\left[\frac{\sqrt{3}}{2}\cos(\theta) - \frac{1}{2}\sin(\theta)\right] \\ V_C &= A_C \sin\left(\theta - \frac{4}{3}\pi\right) = A_C\left[\frac{\sqrt{3}}{2}\cos(\theta) + \frac{1}{2}\sin(\theta)\right] \end{aligned} \tag{1}$$

must be efficiently computed. A sine (and cosine) table of sufficiently small granularity along with numerical interpolation is the most economical way to proceed. The 2nd order interpolation method developed in [5] approximates the in-phase and quadrature-phase terms as[7]

$$\begin{aligned} I &\cong\sim I_{table}\left(1 - \frac{\phi^2}{2}\right) - Q_{table}\phi \\ Q &\cong Q_{table}\left(1 - \frac{\phi^2}{2}\right) + I_{table}\phi \end{aligned} \tag{2}$$

where the angle of interest is given by $\theta = k\,\Delta\theta + \phi$ where the angular step between table look-up values is given by $\Delta\theta$ and $|\phi| \le |\Delta\theta / 2|$. Interpolated performance using (2) versus ideal are shown in Figure 26 through Figure 31 for an effective table lookup length[8] of 160.

[7] Ideally, $I = \cos(\theta)$ and $Q = \sin(\theta)$.

[8] Due to symmetry arguments, the physical lookup table length needs to only be 1/8 of the effective table length.

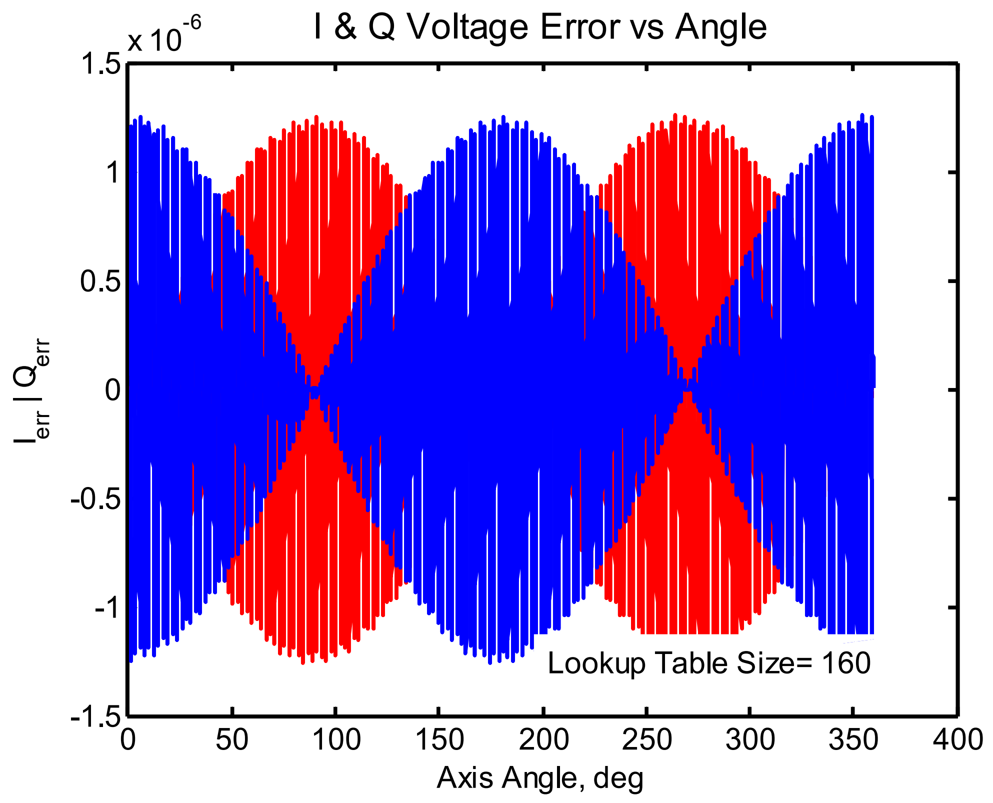

Figure 26 In-phase and quadrature-phase errors

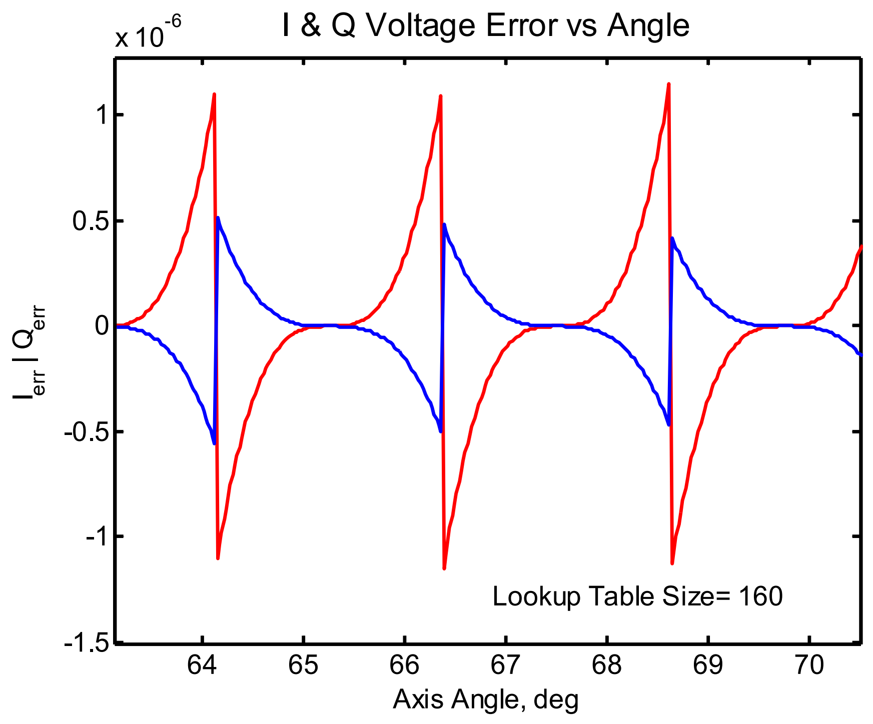

Figure 27 Close-up of Figure 26

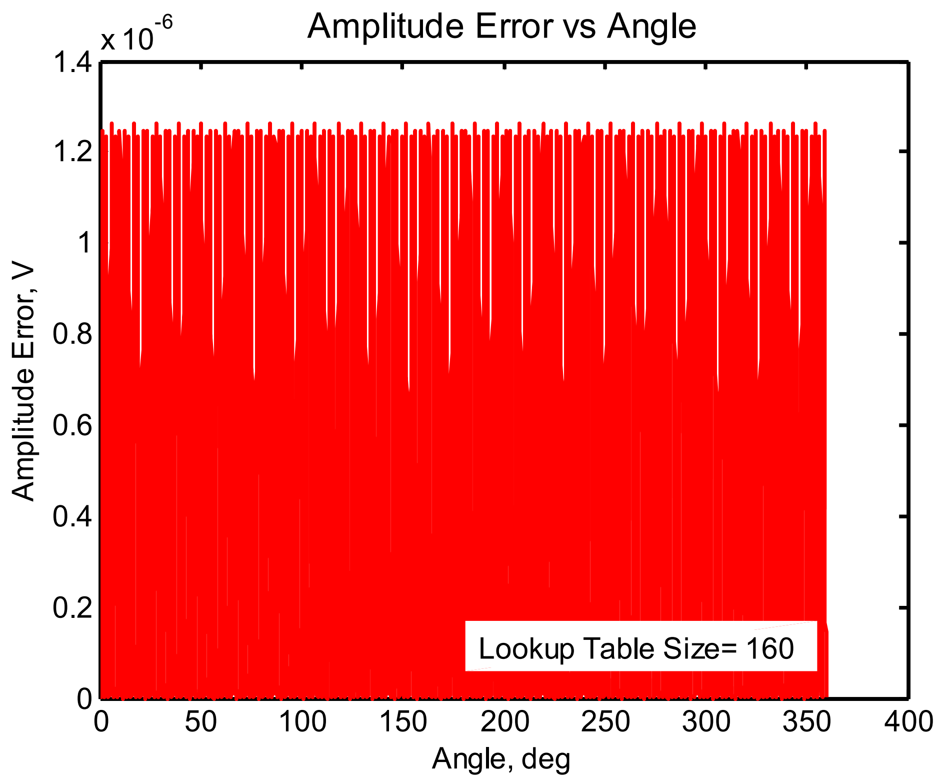

Figure 28 Amplitude error

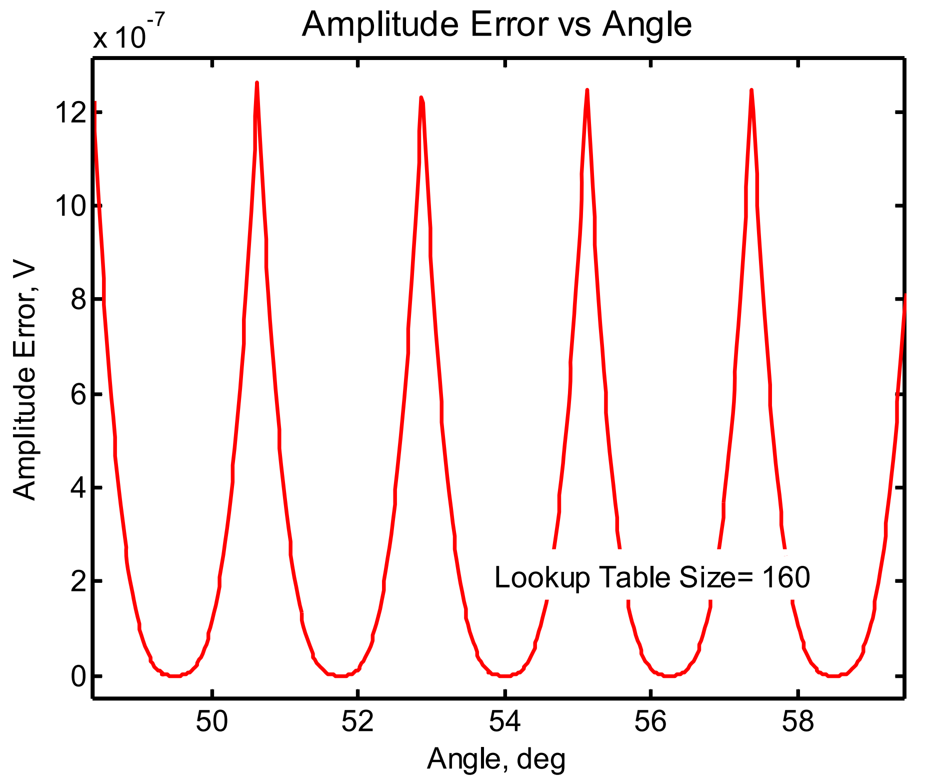

Figure 29 Close-up of Figure 28

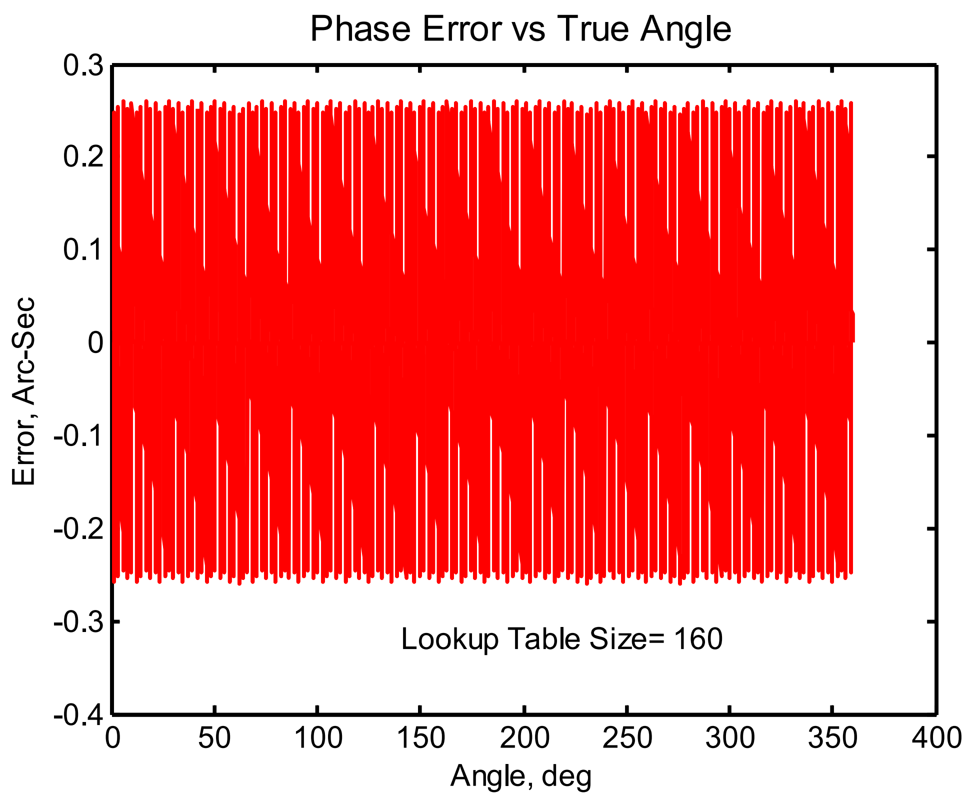

Figure 30 Phase error

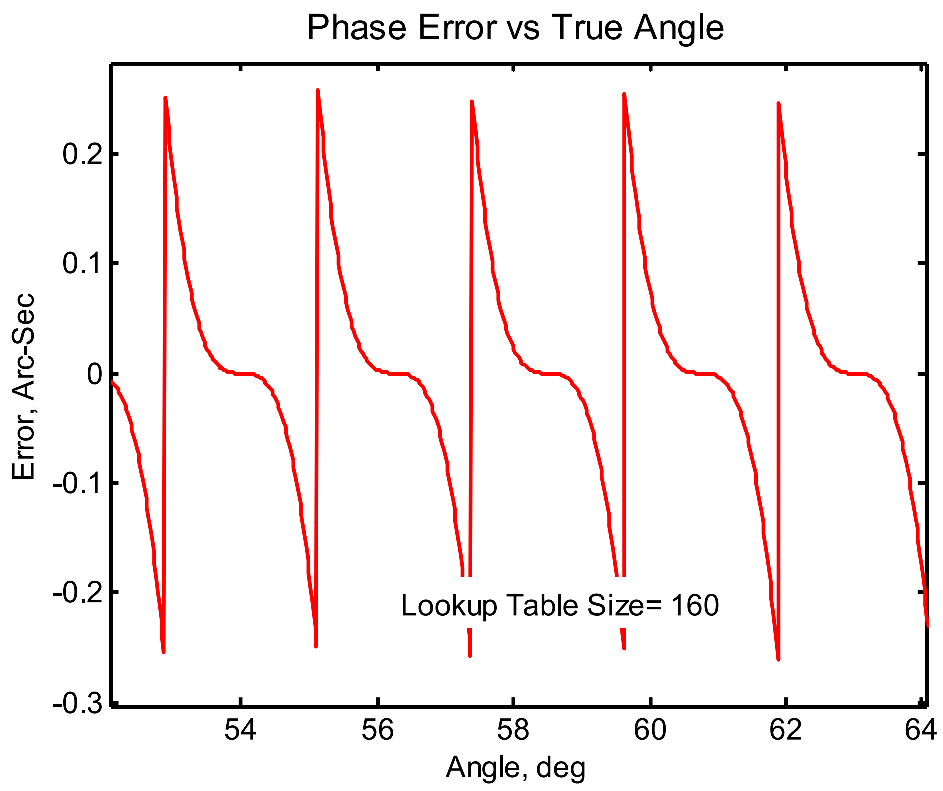

Figure 31 Close-up of Figure 30

Table 4 Interpolation Error Performance vs Table Lookup Size

Effective Lookup Table Size	**Pk-Pk Amplitude Error, V**	**Pk-Pk Phase Error, Arc-Seconds**
64	1.97e-5	8.13
128	2.46e-6	1.02
160	1.26e-6	0.52
192	7.30e-6	0.298
256	3.08e-7	0.127

8 Appendix: IQ Constellation Fidelity & Encoder Precision

As described briefly in §2.2.3, the AEAT-9000 optical encoder delivers 11-bit resolution using Gray-encoded tracks and interpolates the remaining 6-bits using I/Q analog signal interpolation on-chip. The analog I/Q signals are conveyed to the DSP's built-in ADCs and it is these digitized I/Q signals being plotted in Figure 12 and Figure 13. Although the AEAT-9000 datasheet claims that much of the device calibration is done in the factory, an all but undocumented calibration mode is also provided for the device user. It is therefore difficult at best to know the final details with certainty.

If the analog I/Q signals from the AEAT-9000 truly represent the internal state of affairs within the encoder, constellation points are expected to fall onto an ellipse which may also be rotated as well as offset from the origin. An ideal ellipse in the (x, y) plane is given by[9]

$$\frac{x^2}{a^2}+\frac{y^2}{b^2}=1 \tag{3}$$

where the major axis is given by *2a*, the minor axis is given by *2b*, and eccentricity is given by $e = c/a$ along with

$$c=\sqrt{a^2-b^2} \tag{4}$$

Consequently, the eccentricity is also given by

$$e=\frac{c}{a}=\frac{\sqrt{a^2-b^2}}{a}=\sqrt{1-\left(\frac{b}{a}\right)^2} \tag{5}$$

A diagram illustrating the different quantities is provided in Figure 32.

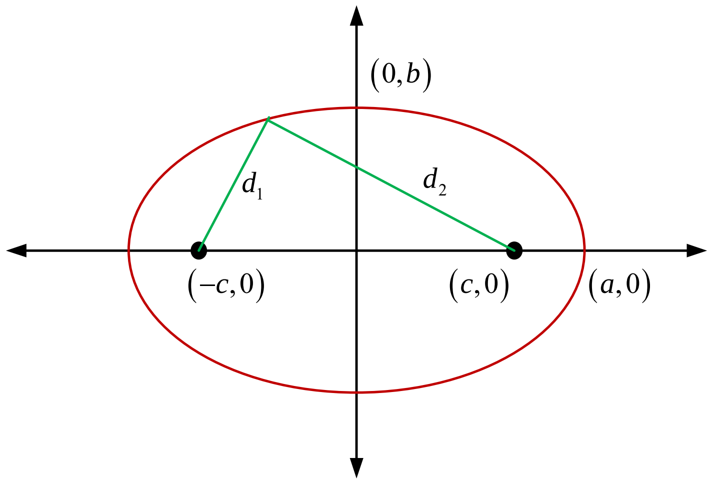

Figure 32 Classic ellipse

If the ellipse (3) is rotated by angle θ and then offset by $(\delta x, \delta y)$, (3) is transformed to

[9] *College Calculus with Analytic Geometry*, Protter & Morrey, 1970, page 303.

$$\frac{\left[x\cos(\theta)-y\sin(\theta)-\delta x\right]^2}{a^2}+\frac{\left[y\cos(\theta)+x\sin(\theta)-\delta y\right]^2}{b^2}=1 \tag{6}$$

Working in reverse with a set of constellation (x, y) points, the best-fit ellipse in terms of *a*, *b*, θ, δx, and δy is now sought. An error function Λ can be defined as

$$\Lambda=\sum_{k=1}^{K}\left\{\frac{\left[x_k\cos(\theta)-y_k\sin(\theta)-\delta x\right]^2}{a^2}+\frac{\left[y_k\cos(\theta)+x_k\sin(\theta)-\delta y\right]^2}{b^2}-1\right\}^2 \tag{7}$$

and the estimation parameters identified which minimizes this function. Subsequent calculations may be somewhat simplified by choosing a modified form of (7) as

$$\Lambda_m=\sum_{k=1}^{K}\left\{b^2\left[x_k\cos(\theta)-y_k\sin(\theta)-\delta x\right]^2+a^2\left[y_k\cos(\theta)+x_k\sin(\theta)-\delta y\right]^2-a^2b^2\right\}^2 \tag{8}$$

This is still too complicated to be used effectively, especially when there will be 2048 interpolation periods involved for the entire encoder wheel. Rather, only a *goodness of alignment* metric (GAM) is being sought from which to guide the encoder's x/y alignment with the axis of rotation. In this respect, a goodness of fit to an ideal circle should be sufficient.

Since the overall control loops will only be making use of the 16-bit digital encoder output, it makes sense to focus the encoder alignment metric on using this output alone. To this end, several assumptions can be made:

- Alignment activities can be done using the DC motor at about 30 RPM, but no lower with the present motor.
- At 30 RPM, the rotation rate is about 0.5 turn per second, resulting in about 1024 I/Q cycles per second.
- At an encoder sampling rate of 160 ksps and capture depth of 200 (I/Q) samples, each capture will encompass only about 1.25 msec and equivalently about one full cycle of the I/Q waveforms.
- Over time intervals of 1.25 msec, mechanical inertia should keep the rotational rate constant even if the motor has some variations (which it no doubt will).
    - The encoder sampling rate can likely be lowered by a factor of 4 to encompass 4 complete I/Q signal cycles without compromising this constant rate assumption.

Under these assumptions, the GAM can be computed for all 2048/4 = 512 segments of the encoder wheel and used to physically align the optical encoder to the axis center as best as possible. If this does still not produce sufficient encoder fidelity, additional compensation methods based upon axle angle will have to be considered.

The GAM for each sample capture will be computed as follows using only the encoder's 16-bit outputs:

1. Estimate the axle's angle corresponding to the center of the capture time. With the constant angular velocity assumption, this is straight forward to do.
2. In a similar fashion, estimate the constant angular velocity present for the capture.
3. Ideally, the angle samples will fall on a straight line. The RMS deviation of samples from the straight line will be the GAM value corresponding to that axle's center position.
4. Subsequent captures are performed until the entire 360° of axle angle travel is characterized in this fashion.